New Journal of Physics
The open access journal at the forefront of physics

Deutsche Physikalische Gesellschaft DPG IOP Institute of Physics

PAPER • OPEN ACCESS

Signatures of superconducting triplet pairing in Ni–Ga-bilayer junctions

To cite this article: Andreas Costa *et al* 2022 *New J. Phys.* **24** 033046

View the article online for updates and enhancements.

You may also like

- Density functional theory study on the interactions of l-cysteine with graphene: adsorption stability and magnetism
Huijuan Luo, Hejun Li, Qiangang Fu et al.
- Hydrogenation of CO_2 on NiGa thin films studied by ambient pressure x-ray photoelectron spectroscopy
Pei-Shun Lin (), Sun-Tang Chang (), Sheng-Yuan Chen () et al.
- Electrochemical Carbon Dioxide Reduction to Hydrocarbons with a Nickel-Gallium Thin Film Catalyst at Low Overpotentials
Sonja A Francis, Daniel A Torelli, J Chance Crompton et al.

This content was downloaded from IP address 91.53.155.66 on 30/03/2022 at 13:12

New Journal of Physics
The open access journal at the forefront of physics

Deutsche Physikalische Gesellschaft DPG
IOP Institute of Physics

Published in partnership with: Deutsche Physikalische Gesellschaft and the Institute of Physics

OPEN ACCESS

RECEIVED
24 November 2021

REVISED
16 February 2022

ACCEPTED FOR PUBLICATION
8 March 2022

PUBLISHED
30 March 2022

Original content from this work may be used under the terms of the Creative Commons Attribution 4.0 licence.

Any further distribution of this work must maintain attribution to the author(s) and the title of the work, journal citation and DOI.

PAPER

Signatures of superconducting triplet pairing in Ni–Ga-bilayer junctions

Andreas Costa[1,*], **Madison Sutula**[2,3], **Valeria Lauter**[4], **Jia Song**[2], **Jaroslav Fabian**[1] **and Jagadeesh S Moodera**[2,5]

[1] Institute for Theoretical Physics, University of Regensburg, 93040 Regensburg, Germany
[2] Francis Bitter Magnet Laboratory and Plasma Science and Fusion Center, Massachusetts Institute of Technology, MA 02139, United States of America
[3] Department of Materials Science and Engineering, Massachusetts Institute of Technology, MA 02139, United States of America
[4] Neutron Scattering Division, Neutron Sciences Directorate, Oak Ridge National Laboratory, Oak Ridge, TN 37831, United States of America
[5] Department of Physics, Massachusetts Institute of Technology, MA 02139, United States of America
[*] Author to whom any correspondence should be addressed.

E-mail: andreas.costa@physik.uni-regensburg.de, lauterv@ornl.gov, jaroslav.fabian@physik.uni-regensburg.de and moodera@mit.edu

Keywords: superconducting triplet pairing, polarized neutron reflectometry, paramagnetic Meissner response

Abstract

Ni–Ga bilayers are a versatile platform for exploring the competition between strongly antagonistic ferromagnetic and superconducting phases. We characterize the impact of this competition on the transport properties of highly-ballistic Al/Al_2O_3(/EuS)/Ni–Ga tunnel junctions from both experimental and theoretical points of view. While the conductance spectra of junctions comprising Ni (3 nm)–Ga (60 nm) bilayers can be well understood within the framework of earlier results, which associate the emerging main conductance maxima with the junction films' superconducting gaps, thinner Ni (1.6 nm)–Ga (30 nm) bilayers entail completely different physics, and give rise to novel large-bias (when compared to the superconducting gap of the thin Al film as a reference) conductance-peak subseries that we term *conductance shoulders*. These conductance shoulders might attract considerable attention also in similar magnetic superconducting bilayer junctions, as we predict them to offer an experimentally well-accessible transport signature of superconducting triplet pairings that are induced around the interface of the Ni–Ga bilayer. We further substantiate this claim performing complementary polarized neutron reflectometry measurements on the bilayers, from which we deduce (1) a *nonuniform magnetization structure* in Ga in a several nanometer-thick area around the Ni–Ga boundary and can simultaneously (2) satisfactorily fit the obtained data only considering the *paramagnetic Meissner response* scenario. While the latter provides independent experimental evidence of induced triplet superconductivity inside the Ni–Ga bilayer, the former might serve as the first experimental hint of its potential microscopic physical origin. Finally, we introduce a simple phenomenological toy model to confirm also from the theoretical standpoint that superconducting triplet pairings around the Ni–Ga interface can indeed lead to the experimentally observed conductance shoulders, which convinces that our claims are robust and physically justified. Arranging our work in a broader context, we expect that Ni–Ga-bilayer junctions could have a strong potential for future superconducting-spintronics applications whenever an efficient engineering of triplet-pairing superconductivity is required.

1. Introduction

Superconducting magnetic junctions form elementary building blocks for superconducting spintronics [1–5], with potential applications in quantum computing [6–13]. Early conductance measurements on ferromagnet/superconductor point contacts [14, 15] demonstrated that Andreev reflection can be used to

© 2022 The Author(s). Published by IOP Publishing Ltd on behalf of the Institute of Physics and Deutsche Physikalische Gesellschaft

quantify the ferromagnet's spin polarization [16]. Nowadays, more complex structures, such as magnetic Josephson-junction geometries [17], in which Yu–Shiba–Rusinov states [18–21] can strongly influence the supercurrent [21, 22] and even induce current-reversing 0–π transitions [23–24], are being exploited. A wealth of unique physical phenomena and transport anomalies has been predicted to emerge in such junctions, covering the potential formation of Majorana states [25–33], significantly magnified current magnetoanisotropies [34–38], as well as the efficient generation and detection of spin-polarized triplet Cooper-pair currents [3, 39].

Particularly appealing materials for superconducting spintronics are Ni–Ga (Ni–Bi) bilayers [40, 41], as strong proximity effects turn the intrinsically weakly ferromagnetic Ni film superconducting. Coexistence of two nominally antagonistic ferromagnetic and superconducting phases in the Ni film can strongly modify transport properties, such as differential conductance. Most remarkable is the possibility of generating spin-triplet states, as previous studies [39, 42–60] drew the conclusion that ferromagnetic exchange can induce odd-frequency superconductivity as a signature of triplet pairing.

The two main factors that cause triplet pairing in proximitized *s*-wave superconductors are inhomogeneously magnetized domains and spin–orbit coupling effects. While triplet currents originating from nonuniform magnetizations have been successfully implemented in various systems [44, 48, 49, 61–69]—e.g., in Nb/Py/Co/Py/Nb junctions through tilting the thin permalloy (Py) spin-mixers' magnetizations [68]—, generating them through spin–orbit coupling could, in certain cases [53, 54], become more challenging and require specific magnetization configurations (relative to the spin–orbit field) to induce sizable enough triplet pairings [70–73].

In this paper, we experimentally investigate the tunneling conductance (dominated by quasiparticles) of high-quality superconducting magnetic Al/Al_2O_3(/EuS)/Ni–Ga junctions that host either thicker Ni (3 nm)–Ga (60 nm) or thinner Ni (1.6 nm)–Ga (30 nm) bilayers. In the latter case, we observe a series of unexpected *conductance shoulders* forming at rather large bias voltages, when compared to the superconducting gap of the thin Al film as a reference, and predict that these conductance shoulders serve as a possible transport fingerprint of superconducting triplet pairings being induced around the Ni–Ga interface. To give independent experimental evidence of this claim, and gain first insights into the potentially underlying physics, we conduct complementary polarized neutron reflectometry (PNR) studies on specific Ni–Ga bilayers, which eventually allow us to visualize the magnetization around the peculiar Ni–Ga boundary. Thereby detecting a nonuniformly magnetized area around the Ni–Ga interface, as well as the *paramagnetic Meissner response* in Ga, provides the key experimental evidence that even weak intrinsic ferromagnetism in Ni can induce a superconducting triplet state [51, 74–77] near the interface of superconducting Ni–Ga bilayers. We further substantiate our findings by means of a a simple phenomenological theoretical toy model that demonstrates that considering superconducting triplet pairings near the Ni–Ga interface is indeed sufficient to qualitatively recover the experimentally observed conductance shoulders. Moreover, we briefly comment on samples with thinner Ni–Ga bilayers that contain an additional, strongly spin-polarized, EuS barrier. The latter is expected to substantially enhance the ferromagnetic exchange interaction inside the junctions, and notably modify their transport characteristics.

We have structured the paper as follows. In section 2, we briefly summarize our state-of-the-art techniques to grow the high-quality superconducting magnetic tunnel junctions, present and discuss the results of our tunneling-conductance measurements carried out on selected samples—paying special attention to the yet puzzling novel large-bias conductance shoulders—, and finally analyze the results of our PNR measurements. Section 3 reports on our theoretical efforts to develop a simple, *purely phenomenological*, description that relates the large-bias conductance shoulders to induced superconducting triplet pairings near the Ni–Ga-bilayer interface. Finally, we briefly conclude our main findings in section 4. Our results might provide an essential contribution to establish Ni–Ga bilayers as promising platforms to engineer spin-polarized triplet supercurrents in future works.

2. Experimental study: conductance features and polarized neutron reflectometry

2.1. Sample growth

All investigated Al/Al_2O_3(/EuS)/Ni–Ga junctions—schematically illustrated in figure 1—with cross-section areas of 150 μm $\times$ 150 μm were prepared by means of thermal evaporation inside an ultra-high vacuum (UHV) system with a base pressure of 2×10^{-8} mb using *in situ* shadow-masking techniques. During the growth process, thin layers of Al, Ni, Ga, and (partly) EuS were evaporated on clean glass substrates kept at temperatures of about 80 K. Ultrathin Al_2O_3 tunneling barriers, separating adjacent Al and (EuS/)Ni–Ga films, were created *in situ* either by exposing Al to a controlled oxygen plasma (producing Al_2O_3 barriers about 1 nm thick) or deposited from an Al_2O_3 source using electron-beam evaporation (to obtain thinner

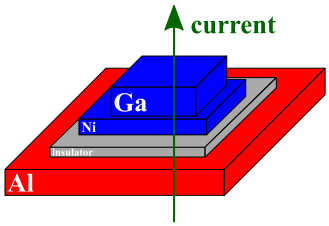

Figure 1. Sketch of the studied Al/insulator [Al_2O_3 (/EuS)]/Ni–Ga junctions. The Al and Ga electrodes are intrinsically superconducting, while proximity effects additionally turn the intrinsically weakly ferromagnetic Ni film likewise superconducting. By applying a bias voltage V between the electrodes and measuring the corresponding tunneling current (indicated by a dark-green arrow), we probe the tunneling-conductance characteristics of the samples.

Table 1. Junction composition of samples A through D. In samples A through C, the Al_2O_3 barriers with a thickness of about 1 nm, separating Al and Ni films, were created by exposing Al to controlled oxygen plasma. In sample D, a 0.4 nm-thick Al_2O_3 barrier was deposited from an Al_2O_3 source using electron-beam evaporation.

Sample A	Al (4 nm)/Al_2O_3 (∼1 nm)/Ni (3 nm)–Ga (60 nm)/Al_2O_3(12 nm)
Sample B	Al(4 nm)/Al_2O_3 (∼1 nm)/Ni(1.6 nm)–Ga(30 nm)/Al_2O_3 (12 nm)
Sample C	Al(4 nm)/Al_2O_3 (∼1 nm)/Ga(30 nm)–Ni(1.6 nm)/Al_2O_3 (12 nm)
Sample D	Al(4 nm)/Al_2O_3 (0.4 nm)/EuS(1.2 nm)/Ni(1.6 nm)–Ga(30 nm)/Al_2O_3 (12 nm)

0.4 nm Al_2O_3 barriers). Before taking the junctions out of the UHV chamber, they were protected by 12 nm-thick Al_2O_3 layers.

In one run, we could prepare several junctions differing only in the thicknesses of individual Al, EuS, Ni, or Ga layers, while keeping all other growth parameters the same. To measure the tunneling conductance, and thus study the ramifications of the superconducting magnetic Ni–Ga bilayers on transport, we attached the junctions to a probe with electrical leads and immersed the system into a pumped liquid-helium bath (either ^{4}He or ^{3}He) to reach a temperature of about 1 K or 0.6 K. Both Al and Ni–Ga thin films turned superconducting, with critical temperatures strongly dependent on their thickness. All our samples were based on 4 nm-thick Al films (serving as the left electrode; note that studying the tunneling conductance requires two distinct superconducting electrodes, which is in stark contrast to STM studies [69] that could probe the Ni–Ga bilayers alone), which have themselves already been intensively investigated in Al/EuS/Al junctions earlier [78] and demonstrated to remain superconducting below a critical temperature of about $T_{\mathrm{Al}}^{\mathrm{crit.}} \approx 2.5$ K; the superconducting coherence length of such thin Al films was estimated by Meservey and Tedrow [79] to be $\xi_{\mathrm{Al}} \approx 50$ nm. Due to the strong competition between ferromagnetism and superconductivity, the critical temperature of the Ni–Ga bilayers (serving as the right electrode) is mostly determined by the thickness of the Ni film, and usually drops down with increasing Ni thickness (stronger ferromagnetic exchange). At about 2 nm Ni, the critical temperature of the Ni–Ga bilayer is roughly $T_{\mathrm{Ni-Ga}}^{\mathrm{crit.}} \approx 4.2$ K; typical superconducting coherence lengths of Ni (0.4 nm)–Ga (14 nm) bilayers are of the order of $\xi_{\mathrm{Ni-Ga}} \approx 15$ nm [40]. Performing Meservey–Tedrow spectroscopy [79–81], we further estimated that the weak intrinsic ferromagnetic exchange within thin Ni films causes spin polarizations of about 1%, which noticeably increase above 4 nm Ni thickness.

2.2. Tunneling-conductance measurements

To demonstrate the most puzzling transport features of Ni–Ga-bilayer junctions that we could detect in our series of experiments, we focus on four different samples (labeled *sample A* through *sample D*; see table 1) containing either a thicker Ni (3 nm)–Ga (60 nm) or a thinner Ni (1.6 nm)–Ga (30 nm) bilayer, respectively. All tunneling-conductance data was obtained using standard lock-in technique.

Sample A. First, we studied the Al (4 nm)/Al_2O_3 (∼1 nm)/Ni (3 nm)–Ga (60 nm)/Al_2O_3 (12 nm) junction with a thicker Ni (3 nm)–Ga (60 nm) bilayer and at a temperature of about 1.1 K. The results of our measurements, which are shown in figure 2, reveal three distinct *main* (first-order) conductance maxima.

The quasiparticle tunneling conductance of similar (Josephson-like) junction geometries, consisting of two superconducting electrodes that are separated by a thin nonsuperconducting link, has already been intensively investigated in numerous systems and by several authors before (see, e.g., references [82–92]). Rowell and Feldman [89, 91] developed thereby one of the perhaps most fundamental theoretical descriptions of these S/N/S′ junctions' tunneling conductance, assuming two *dissimilar* superconducting electrodes S and S′ connected by a thin nonsuperconducting N link. Their Rowell–Feldman approach

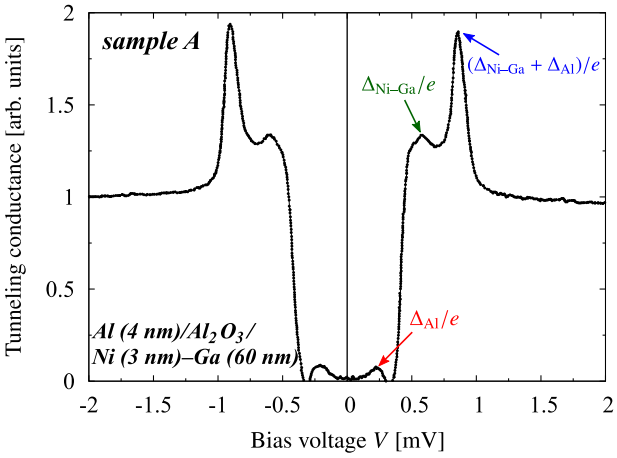

Figure 2. The *measured* tunneling conductance–bias voltage characteristics of the Al (4 nm)/Al_2O_3 (∼1 nm)/Ni (3 nm)–Ga (60 nm)/Al_2O_3 (12 nm) junction, with a thicker Ni (3 nm)–Ga (60 nm) bilayer, at a temperature of about 1.1 K. The positions (bias voltages) of the *main* conductance peaks (maxima) are determined by the superconducting gaps of the left Al electrode, Δ_{Al}, and the right Ni–Ga-bilayer electrode, Δ_{Ni-Ga}, as indicated.

predicts the emergence of *main* conductance peaks whenever the applied bias voltage V satisfies $eV \approx \mp\Delta_{S'}$, $eV \approx \mp(\Delta_S + \Delta_{S'})$, or $eV \approx \mp\Delta_S$, where Δ_S ($\Delta_{S'}$) denotes the superconducting gap of S (S′) and e refers to the positive elementary charge. At the microscopic level, Arnold [93, 94] related the appearance of these conductance peaks to multiple Andreev reflections that occur at these particular bias voltages.

Interestingly, we can directly adapt the predictions of the Rowell–Feldman model to understand the conductance features that we observed in sample A (see figure 2). We identify the thin Al film on the left- and the Ni–Ga bilayer on the right-hand side as the superconducting electrodes S and S′ of our samples, while the thin Al_2O_3 tunneling barrier serves as the nonsuperconducting link. From the main conductance peaks (maxima) displayed in figure 2, we can therefore estimate the superconducting gaps of Al, Δ_{Al}, and Ni–Ga, Δ_{Ni-Ga}, such that the conductance maxima arise at $eV \approx \mp\Delta_{Al}$, $eV \approx \mp\Delta_{Ni-Ga}$, and $eV \approx \mp(\Delta_{Al} + \Delta_{Ni-Ga})$, accordingly. At a temperature of about 1.1 K, at which the conductance measurements were performed, we finally obtain $\Delta_{Al} \approx 0.25$ meV—which is in good agreement with such thin Al films' (zero-temperature) gap of about 0.36 meV [40]—as well as $\Delta_{Ni-Ga} \approx 0.6$ meV; the latter might be compared to the gap of an earlier studied Ni (2 nm)–Ga (100 nm) bilayer [40], which was estimated to be about 0.57 meV and is one of the rare references of Ni–Ga bilayers that are available in the literature. Since the Rowell–Feldmann approach suffices to satisfactorily explain the conductance features of sample A, and extract physically reasonable values of the Al and Ni–Ga-bilayer electrodes' superconducting gaps, we might conclude already at this point that the ferromagnetic exchange inside Ni does not *substantially* affect the physics of the thicker Ni (3 nm)–Ga (60 nm) bilayer; recall that Rowell and Feldman did not account for ferromagnetic components. We will in fact see later on that the interface magnetization of thicker Ni–Ga bilayers remains more uniform and, most likely due to their simultaneously weak spin polarizations of just about 1%, the Ni films' ferromagnetism does consequently not yet raise novel physics in thicker Ni (3 nm)–Ga (60 nm) bilayers.

Samples B and C. The second and third samples that we investigated were composed of the Al (4 nm)/Al_2O_3 (∼1 nm)/Ni (1.6 nm)–Ga (30 nm)/Al_2O_3 (12 nm) junction with a thinner Ni (1.6 nm)–Ga (30 nm) bilayer and the Al (4 nm)/Al_2O_3 (∼1 nm)/Ga (30 nm)–Ni (1.6 nm)/Al_2O_3 (12 nm) junction with an effectively '*inverted*' Ga (30 nm)–Ni (1.6 nm) bilayer, respectively. The corresponding tunneling conductances measured at a temperature of about 1.1 K, which are shown in figure 3, reflect much richer conductance features than before (in sample A).

Specifically, each of the two large-bias (taking the gap of the thin Al film as the smallest energy reference in the system) conductance maxima that we associated with Δ_{Ni-Ga} and $\Delta_{Ni-Ga} + \Delta_{Al}$ in sample A seems to split into a subseries of (at least) two distinct and individually resolvable conductance maxima, which we will call *conductance shoulders* hereinafter. These conductance shoulders have not yet been explored in prior works; providing a sophisticated picture of their physical origin is therefore the main objective of our paper.

As the conductance shoulders only arise in junctions with thinner Ni–Ga bilayers, they are most likely intimately connected with novel physical phenomena that solely arise in thinner Ni–Ga bilayers. In our earlier theoretical work on the transport characteristics of ferromagnet/superconductor/ferromagnet junctions in the presence of interfacial spin–orbit interactions [95], we identified splittings of main

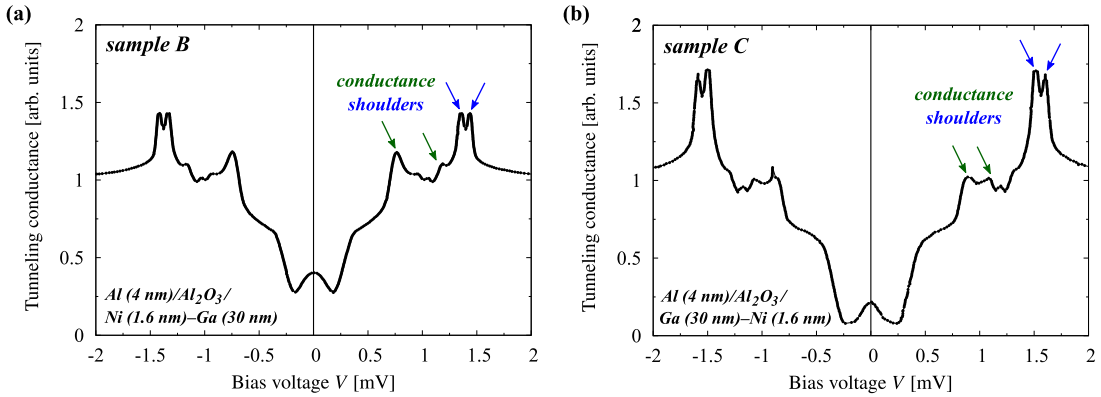

Figure 3. (a) The *measured* tunneling conductance–bias voltage characteristics of the Al (4 nm)/Al_2O_3 (∼1 nm)/Ni (1.6 nm)–Ga (30 nm)/Al_2O_3 (12 nm) junction, with a thinner Ni (1.6 nm)–Ga (30 nm) bilayer, at a temperature of about 1.1 K. (b) The same measurement as in (a), but replacing the Ni (1.6 nm)–Ga (30 nm) bilayer by an '*inverted*' Ga (30 nm)–Ni (1.6 nm) bilayer. Note that the large-bias conductance maxima, discussed in figure 2, are divided into a series of conductance shoulders indicated by green and blue arrows; each shoulder consists of (at least) two individually resolvable adjacent conductance maxima.

conductance peaks into a shoulder-like pattern as signatures of 'unconventional' (i.e., spin-flip) Andreev reflections at the interfaces. These unconventional Andreev reflections effectively induce superconducting triplet pairings in the junction. From that point of view, the large-bias conductance shoulders occurring in junctions with thinner Ni (1.6 nm)–Ga (30 nm) bilayers *might* likewise provide transport fingerprints of superconducting triplet pairings. Nevertheless, before we can safely establish a connection between conductance shoulders and triplet superconductivity, we need to provide clear experimental evidence of the latter—which we will when analyzing the results of our PNR measurements.

Furthermore, the conductance data of samples B and C also reveal clearly visible zero-bias conductance peaks, which we did not detect in sample A with the thicker Ni (3 nm)–Ga (60 nm) bilayer. Deducing the physical mechanism that causes such zero-bias peaks is usually a highly nontrivial task, as they could stem from numerous distinct phenomena—like, for example, zero-energy Andreev reflections [96, 97] or, as well *in some cases*, superconducting triplet pairings [98, 99]. More specifically, a previous experimental study [98] demonstrated that unexpectedly pronounced zero-bias conductance peaks (with amplitudes even exceeding those of their normal-state counterparts) arising in the tunneling conductance of superconductor/half-metal bilayers may be indicative of triplet superconductivity. At the microscopic level, inhomogeneous magnetizations around the interface can flip some of the Cooper-pair electrons' spins, and thereby generate a 'mixture' of spin-singlet and spin-triplet components in the superconducting order parameter [44, 48, 49, 61–69, 98–102].

In bilayers that contain not fully spin-polarized ferromagnets (i.e., no half metals as the second electrode), the situation might be much more intriguing. Thoroughly investigating electrical transport through Al/EuS bilayers, Diesch *et al* [69] revealed that—instead of a single zero-bias conductance peak—superconducting triplet pairings give then rather rise to a rich, and not necessarily symmetric with respect to zero bias, low-bias double-peak conductance pattern, in which the gap between the two newly forming conductance peaks could be connected to the strength of the induced triplet pairings. Within the applied STM techniques, it was furthermore possible to individually address different transverse channels of the Al/EuS-bilayer junctions. As a result, Diesch and coworkers proposed that the magnetization around the Al/EuS interface is indeed inhomogeneous (on a length scale of a few nanometers, which could refer to the grain size of thin EuS films), which is again most likely the mechanism that is responsible for the aforementioned 'mixing' of singlet and triplet order parameters.

Coming back to samples B and C of our study, we must therefore conclude that the appearance of zero-bias conductance peaks alone is neither a unique nor a sufficient signature of superconducting triplet pairings, and might as well originate from different physical effects. However, as the main focus of our work is to understand the peculiar large-bias conductance shoulders, and interpret these as clear fingerprints of triplet pairings, we did not further analyze the zero-bias peaks.

As another remarkable experimental feature, our conductance measurements on samples B and C suggest that replacing the Ni (1.6 nm)–Ga (30 nm) by a Ga (30 nm)–Ni (1.6 nm) bilayer—i.e., inverting the order of the Ni and Ga films inside the bilayers—has no substantial effect on the large-bias conductance shoulders [see figures 3(a) and (b)]. We take this finding as an experimental hint that the physics being responsible for the formation of large-bias conductance shoulders occurs *around the Ni–Ga interface*, and is thus quite independent of the order of the Ni and Ga films. Together with our claim that the conductance

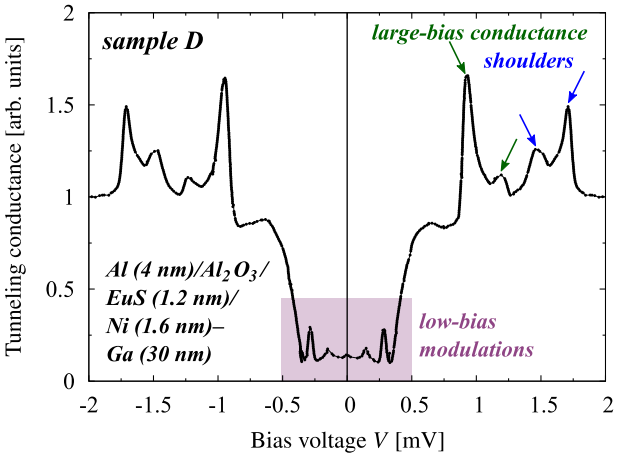

Figure 4. The *measured* tunneling conductance–bias voltage characteristics of the Al (4 nm)/Al_2O_3 (0.4 nm)/EuS (1.2 nm)/Ni (1.6 nm)–Ga (30 nm)/Al_2O_3 (12 nm) junction, with a thinner Ni (1.6 nm)–Ga (30 nm) bilayer, at a temperature of about 1 K. Green and blue arrows indicate the large-bias conductance shoulders, whereas the purple shaded low-bias regime reveals much richer conductance modulations than a similar junction without the EuS barrier [recall figure 3(a)].

shoulders signify superconducting triplet pairings, we could therefore argue that the physical mechanism inducing triplet correlations in Ni–Ga bilayers could be similar to the aforementioned ones; i.e., the magnetization around the interface of Ni (1.6 nm)–Ga (30 nm) bilayers is inhomogeneous (on a length scale of a few nanometers), which partially converts spin-singlet into spin-triplet Cooper pairs through flipping some of the electrons' spins. Nonetheless, this interpretation certainly requires more pertinent experimental evidence, which we will provide within our PNR measurements that are directly able to probe the profile of the interface magnetizations and thereby support our predictions.

Sample D. As the thin Ni films of our junctions are only weakly ferromagnetic (recall that we deduced spin polarizations of about 1% from Meservey–Tedrow spectroscopy)—and the triplet-pairing effects are thus most likely also rather moderate—, a more promising perspective could be to focus on samples that contain a second strongly ferromagnetic component. The fourth studied sample consisted therefore of the Al (4 nm)/Al_2O_3 (0.4 nm)/EuS (1.2 nm)/Ni (1.6 nm)–Ga (30 nm)/Al_2O_3 (12 nm) junction, which basically corresponds to sample B except for the additional 1.2 nm-thick barrier composed of the strong ferromagnetic insulator EuS [103, 104]. Such barriers have attracted considerable attention after earlier works [78, 105] had demonstrated that their high spin-filtering efficiency indeed provides an experimentally well-controllable way to convert more singlet into triplet Cooper pairs, and thereby generate (almost) completely spin-polarized triplet supercurrents.

The tunneling conductance of sample D at a temperature of about 1 K is presented in figure 4.

As the most important feature, we assert that the large-bias conductance shoulders—which we claimed to signify superconducting triplet pairings at the Ni–Ga interface—are robust and even slightly more pronounced than in samples B and C (i.e., the splittings between the shoulders' conductance maxima are slightly larger). This observation could be carefully interpreted as a possible experimental hint that the additional ferromagnetic EuS spacer may indeed amplify the triplet pairings. Moreover, adding EuS gives rise to extremely rich low-bias conductance modulations that we could not detect in samples A through C in which EuS was absent. As we pointed out previously, STM studies of Al/EuS bilayers performed by Diesch *et al* [69] indicated that low-bias conductance double peaks (rather than just a single zero-bias conductance peak) could provide another signature of interfacial triplet pairings. Our results obtained from sample D look physically similar, apart from detecting four instead of two low-bias peaks (two at negative and two at positive voltages, respectively). Analogously to the zero-bias peaks of samples B and C, unraveling the physical origin of these low-bias features has not yet been possible with the available data, and goes also beyond the scope of this manuscript. One possible explanation for the doubling of low-bias peaks (when compared to Diesch's work) might be that we are dealing with two different ferromagnetic films—EuS *and* Ni—instead of just one (EuS) as Diesch and coworkers, and thus need to consider two distinct interfaces at which the magnetization may be inhomogeneous. However, this is a premature statement that we cannot uniquely confirm from our measurements.

2.3. Polarized neutron reflectometry

While discussing the tunneling-conductance data obtained from samples B and C in the preceding section, we argued that the observed large-bias conductance shoulders might serve as an experimentally accessible

transport signature of superconducting triplet pairings getting induced by inhomogeneous magnetizations around the interface of thinner Ni (1.6 nm)–Ga (30 nm) bilayers. In the following, we wish to provide *independent* experimental evidence of this claim through a deeper characterization of the physical properties of this peculiar interface.

For a deeper investigation of the Ni–Ga interface, and to directly explore its structure and magnetization depth profile, we combine depth-sensitive PNR with low-angle x-ray reflectometry (XRR) studies. Being electrically neutral, spin-polarized neutrons penetrate the entire multilayer junctions, probing the magnetic and structural composition of their films through buried interfaces down to the substrate [106]. PNR allows for a direct determination of both the absolute value and the direction of the magnetic field induced inside the superconductor and was previously successfully applied to observe the diamagnetic Meissner effect, as well as vortex-line distributions, in niobium- and YBCO-bilayer films [107, 108]. In this paper, we report on the detection of *inhomogeneous interface magnetizations* and the *paramagnetic Meissner effect* in superconducting Ga, which altogether confirm our earlier claims that the proximity coupling in the Ni–Ga bilayer indeed induces superconducting triplet states [51, 74–77, 109] near the interface, appearing to be responsible for the experimentally observed large-bias conductance shoulders. The PNR experiments were performed on the Magnetism Reflectometer at the Spallation Neutron Source at Oak Ridge National Laboratory [107, 110], using a neutron beam with a wavelength band $\Delta\lambda$ of 2.6–8.6 Å; and high polarization of 98.5% to 99%. After cooling in zero field (ZFC), measurements were conducted at temperatures of 15 K and 5 K, with an external magnetic field applied in the plane of the sample up to 0.1 T. Using the time-of-flight method, a collimated polychromatic beam of polarized neutrons with a wavelength band $\Delta\lambda$ impinges on the film at a grazing incidence angle θ, where it interacts with atomic nuclei and the spins of unpaired electrons. Then, the reflected intensity is measured as a function of the wave-vector transfer $Q = 4\pi \sin\theta/\lambda$ for two neutron polarizations R^+ and R^- with the neutron spin parallel $(+)$ or antiparallel $(-)$ to the direction of the external field $H_{\text{ext.}}$; λ denotes the neutron wavelength. To separate nuclear from magnetic scattering, we present our data in terms of the spin-asymmetry ratio $\text{SA} = (R^+ - R^-)/(R^+ + R^-)$. For example, a value of $\text{SA} = 0$ means that there is no magnetic moment in the system. The depth profiles of the *nuclear* and *magnetic scattering length densities* (*NSLD* and *MSLD*) correspond to the depth profiles of the chemical and in-plane magnetization vector distributions, respectively. The total magnetization M can be calculated from the MSLD data using the relation $M(\text{emu/cm}^3) = \text{MSLD}(\text{Å}^{-2})/(2.853 \times 10^{-9})$.

To verify the depth morphology of the films, we used complementary XRR data. These experiments were carried out on Ni–Ga bilayers with the Ga thickness fixed at about 25 nm (fitting our data, we obtain 21 nm Ga thickness), while the Ni thickness was varied to cover 0.8 nm, 2.4 nm, 4.0 nm, and 5.6 nm; see figure 5. These bilayers are comparable (in film thicknesses) to those in samples B and C, which let the puzzling large-bias conductance shoulders occur. We explored the behavior of the magnetization of the bilayers above and below their critical temperature. The samples were investigated under the same conditions as above, starting with ZFC down to 15 K and measuring at 0.1 T. After that, the magnetic field was turned off, the sample was cooled to 5 K, and the measurement was repeated at a magnetic field of 0.1 T. The sample with the 5.6 nm-thick Ni film showed a clear magnetic signal [i.e., clear SA splitting between reflectivity for neutrons with spin up (R^+) and spin down (R^-)]. For the sample containing the 4.0 nm-thick Ni film, the SA magnetic signal was reduced by a factor of 3, while no measurable magnetization could be detected (within the accuracy of this method) for the samples with the 2.4 nm- and 0.8 nm-thick Ni films. NSLD and MSLD depth profiles were obtained by simultaneous fitting to PNR and XRR data (shown in figure 6), and finally plotted as a function of depth from the surface (see figure 7) for the sample with the 5.6 nm-thick Ni film.

To analyze the electromagnetic proximity effect in Ni–Ga-bilayer structures from the PNR data, we distinguish between two scenarios: (1) the conventional *diamagnetic Meissner screening* and (2) the *paramagnetic Meissner response* in Ga. The results for both cases are shown in figure 7. Fitting the PNR (obtained at 5 K, which is below that bilayer's superconducting critical temperature) and XRR data, we observe that the Ni (5.6 nm)–Ga (25 nm) interface is sharp with a roughness of 0.5 nm. The thickness of the Ga layer refined by the fit is 21 nm. The PNR spin-asymmetry ratio $\text{SA} = (R^+ - R^-)/(R^+ + R^-)$ reveals that the best fit to the data requires 68 emu/cm^3 induced magnetization over roughly 7 nm in Ga in the vicinity of the Ni–Ga interface, while the magnetization in the Ni film is about 164 emu/cm^3 and uniform. For comparison and confirmation of our findings, we additionally consider the model of *diamagnetic Meissner screening* with a penetrating flux. In this case, the MSLD profile will have a contribution from the magnetic field penetration depth from both interfaces of the film. Given that the Ga layer is only 21 nm thick, the magnetic field penetrates the entire film [111] so that the diamagnetic effect is significantly reduced [see dashed line in figure 7(b)] and the corresponding SA in figure 7(a) shows considerable deviations from the experimental points. We are thus able to directly see the induced

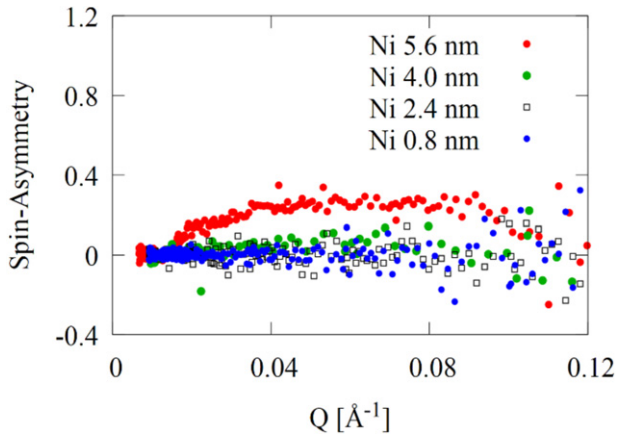

Figure 5. Polarized neutron reflectometry (PNR) results for Ni–Ga (25 nm) bilayers with various Ni thicknesses. Spin-asymmetry ratio SA $= (R^+ - R^-)/(R^+ + R^-)$ obtained from the experimental reflectivity for spin-up (R^+) and spin-down (R^-) neutron spin states shown as a function of wave-vector transfer $Q = 4\pi \sin\theta/\lambda$, where θ indicates the incident angle and λ is the neutron wavelength.

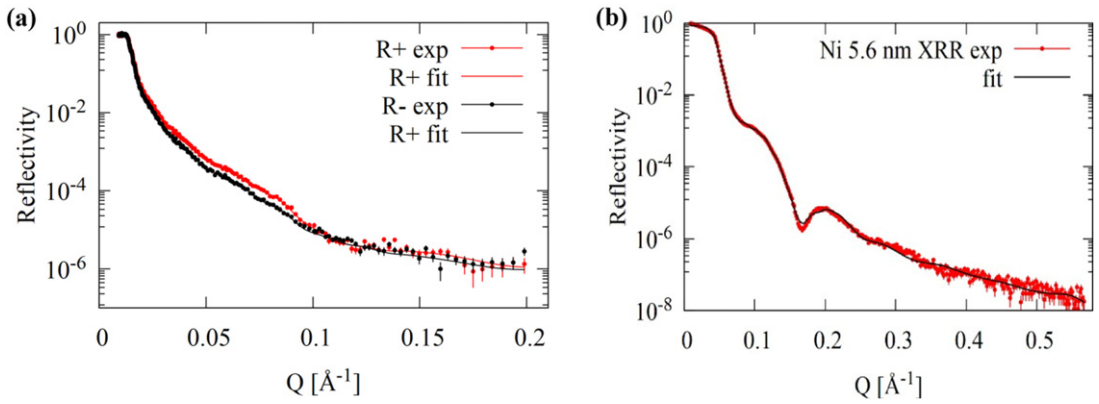

Figure 6. Polarized neutron reflectometry (PNR) and x-ray reflectometry (XRR) results for the Ni (5.6 nm)–Ga (25 nm) bilayer. (a) Experimental reflectivity as a function of the wave-vector transfer Q for spin-up (R^+) and spin-down (R^-) neutron spin states measured in 0.1 T after a zero-field cooling to 5 K. (b) Complementary XRR data has been used to verify the films' depth morphology. The chemical and magnetization depth profiles obtained from the fit to the data are shown in figure 7. From the fit to the PNR and XRR, we deduce that the Ni (5.6 nm)–Ga (25 nm) interface is sharp with a roughness of 0.5 nm. The Ga layer's density is not uniform and consists of two roughly 7 nm- and 18 nm-thick sublayers (see also figure 7).

ferromagnetic order's influence inside the Ga layer *right at the interface* with the Ni film, which should be attributed to the *paramagnetic Meissner response*. Therefore, PNR provides strong *independent* experimental evidence [51, 74–77] of our claims that inhomogeneous magnetizations induce superconducting triplet pairings near the interface of the Ni–Ga bilayer.

To better illustrate the impact of the thickness of the Ni film on the interface and magnetization structure, we analyze the PNR data obtained from Ni–Ga bilayers with 4 nm, 2.4 nm, and 0.8 nm Ni films (recall figure 5) in a similar manner; the thickness of Ga is still 25 nm. From these data analyses, presented in figure 8, we could indeed detect a significant difference between the structural (nonmagnetic) and the magnetic Ni–Ga interface roughness. While the structural interfacial roughness is about 0.5 nm for 5.6 nm-thick Ni, we extract 1.5 nm roughness for 4 nm-, 2.4 nm-, and 0.8 nm-thick Ni, respectively. From the PNR measurements performed at 0.1 mT magnetic field and 15 K temperature, we deduce that the interfacial magnetization is inhomogeneous and extending over several nanometers of 7 nm, 8 nm, and 9 nm (for 5.6 nm-thick, 4 nm-thick, and 2.4 nm-thick Ni). For the bilayer containing 0.8 nm Ni, the accuracy of our approach does not suffice to resolve the magnetization profile. As a more inhomogeneous interface magnetization is expected to convert more spin-singlet into spin-triplet Cooper pairs to enhance the triplet-pairing mechanism, it could thus be promising to explore as a next step the tunneling conductance of bilayers altering the thickness of the Ni film (and keeping Ga the same). Increasing the Ni thickness might then suppress and decreasing the Ni thickness further amplify the triplet pairings, and therefore the conductance shoulders shall become either less or more pronounced.

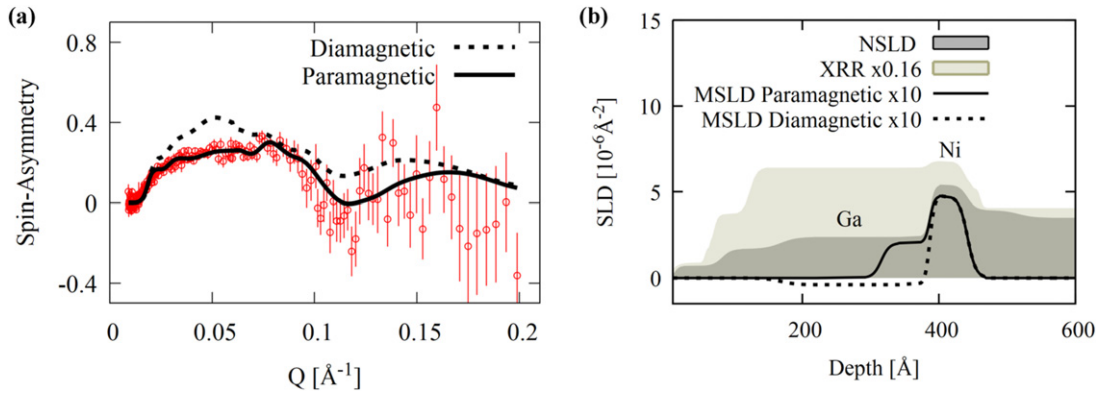

Figure 7. Polarized neutron reflectometry (PNR) results for the Ni (5.6 nm)–Ga (25 nm) bilayer. (a) PNR spin-asymmetry ratio $SA = (R^+ - R^-)/(R^+ + R^-)$; the best fit to the data corresponds to the magnetization profile shown as the solid black line in (b)—i.e., to the *paramagnetic Meissner state*—, revealing 68 emu/cm^3 induced magnetization over about 7 nm in Ga, while the Ni film's magnetization is about 164 emu/cm^3 and uniform. In contrast, the diamagnetic Meissner state in the spin-asymmetry (SA) plot and its magnetic scattering-length density (MSLD) profile, referring to the dashed black lines, notably deviate from the experimental data.

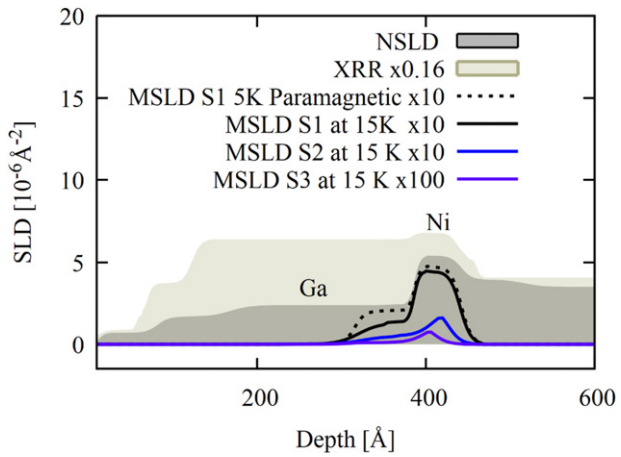

Figure 8. Polarized neutron reflectometry (PNR) results (see figure 7 for details) for Ni–Ga (25 nm) bilayers with 5.6 nm (S1), 4 nm (S2), and 2.4 nm (S3) Ni films. For 0.8 nm Ni (S4), we could not detect a net magnetization within the accuracy of our measurement.

3. Theoretical toy model: large-bias conductance shoulders as signatures of interfacial triplet pairings

As we outlined in section 2 when discussing our experimental results, the appearance of large-bias shoulders in the tunneling conductance of Ni–Ga bilayers can serve as a signature of superconducting triplet pairings induced at the Ni–Ga interface—microscopically originating from inhomogeneous interface magnetizations, as our PNR analyses clearly demonstrated. In this final section of our paper, we formulate a purely phenomenological toy model to *theoretically* convince *at the qualitative level* that superconducting triplet pairings at the Ni–Ga interface give indeed rise to the experimentally detected large-bias conductance shoulders.

3.1. Phenomenological toy model

To describe quasiparticle excitations in Al/Ni–Ga junctions (for simplicity, our toy model neglects the Al_2O_3 tunneling barriers), we formulate their Bogoliubov–de Gennes Hamiltonian [112] on a lattice and compute the tunneling DOS at zero temperature using the Python transport package Kwant [113]. For simplicity, we consider a two-dimensional square lattice with spacing $a = 1$ [arb.units] between two adjacent lattice sites; each site with the real-space coordinates $(z, y) = (ai, aj)$ is uniquely identified by its integer lattice indices (i, j). Figure 9(a) shows a graphical representation of the chosen tight-binding lattice. We denote the numbers of lattice sites along the longitudinal $\hat{z}$-direction inside the Al, Ni, and Ga junction

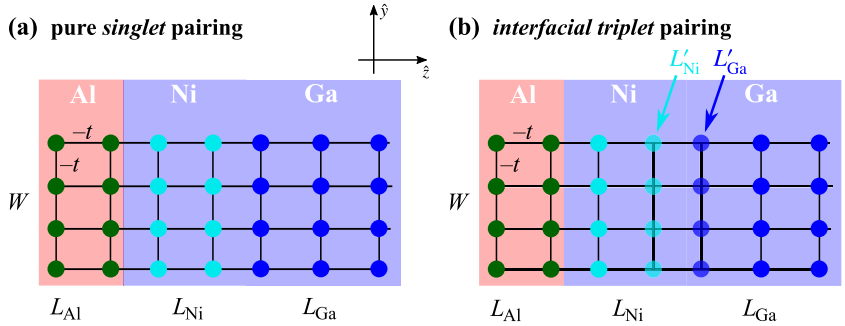

Figure 9. (a) Schematic representation of the Al/Ni–Ga junctions' tight-binding modeling within the Kwant Python transport package, starting with a square lattice with the constant spacing $a = 1$ [arb.units]. The numbers of horizontal lattice sites inside the junctions' different regions are denoted by L_{Al}, L_{Ni}, and L_{Ga}, respectively, and that along the transverse direction by W. The colored dots represent the *on-site energies*, determined by the Bogoliubov–de Gennes Hamiltonian stated in equation (1), while t measures the strength of the *nearest-neighbor hoppings*. All superconducting gaps (pairing potentials) capture only pure singlet pairings. (b) Same as in (a), but assuming that the superconducting gaps (pairing potentials) in Ni and Ga combine singlet with *triplet* pairings within the L'_{Ni} and L'_{Ga} lattice sites around their interface.

regions by L_{Al}, L_{Ni}, and L_{Ga}, respectively, whereas we assume in total W lattice sites along the transverse $\hat{y}$-direction.

The *on-site energies* (with respect to the Fermi level) at lattice site (i, j) are then given by the discretized Nambu-space Bogoliubov–de Gennes Hamiltonian [$\Theta(\ldots)$ denotes the Heaviside step function]

$$\begin{aligned}\hat{\mathcal{H}}_{\mathrm{BdG}}(i,j) = \Big[& 4t\,\hat{\tau}_0 + \Delta_{\mathrm{Al}}^{\mathrm{singlet}}\,\hat{\tau}_2\,\Theta(i)\,\Theta(L_{\mathrm{Al}} - i) \\ & + \Delta_{\mathrm{Ni}}^{\mathrm{XC}}\,\hat{\tau}_1\,\Theta(i - L_{\mathrm{Al}} - 1)\,\Theta(L_{\mathrm{Al}} + L_{\mathrm{Ni}} - i) \\ & + \Delta_{\mathrm{Ni-Ga}}^{\mathrm{singlet}}\,\hat{\tau}_2\,\Theta(i - L_{\mathrm{Al}} - 1)\,\Theta(L_{\mathrm{Al}} + L_{\mathrm{Ni}} - i) \\ & + \Delta_{\mathrm{Ni-Ga}}^{\mathrm{triplet}}\,\hat{\tau}_3\,\Theta(i - L_{\mathrm{Al}} - L_{\mathrm{Ni}} + L'_{\mathrm{Ni}} - 1)\,\Theta(L_{\mathrm{Al}} + L_{\mathrm{Ni}} - i) \\ & + \Delta_{\mathrm{Ni-Ga}}^{\mathrm{singlet}}\,\hat{\tau}_2\,\Theta(i - L_{\mathrm{Al}} - L_{\mathrm{Ni}} - 1)\,\Theta(L_{\mathrm{Al}} + L_{\mathrm{Ni}} + L_{\mathrm{Ga}} - i) \\ & + \Delta_{\mathrm{Ni-Ga}}^{\mathrm{triplet}}\,\hat{\tau}_3\,\Theta(i - L_{\mathrm{Al}} - L_{\mathrm{Ni}} - 1)\,\Theta\left(L_{\mathrm{Al}} + L_{\mathrm{Ni}} + L'_{\mathrm{Ga}} - i\right)\Big] \\ & \times \Theta(j)\,\Theta(W - 1 - j), \end{aligned} \tag{1}$$

and the *nearest-neighbor hoppings* ($\langle i, j\rangle$ indicates nearest-neighbor lattice sites) by

$$\hat{\mathcal{H}}_{\mathrm{hop}}(\langle i,j\rangle) = -t\,\hat{\tau}_0, \tag{2}$$

where

$$\hat{\tau}_0 = \begin{bmatrix} 1 & 0 & 0 & 0 \\ 0 & 1 & 0 & 0 \\ 0 & 0 & -1 & 0 \\ 0 & 0 & 0 & -1 \end{bmatrix}, \qquad \hat{\tau}_1 = \begin{bmatrix} 1 & 0 & 0 & 0 \\ 0 & -1 & 0 & 0 \\ 0 & 0 & 1 & 0 \\ 0 & 0 & 0 & -1 \end{bmatrix}, \qquad \hat{\tau}_2 = \begin{bmatrix} 0 & 0 & 1 & 0 \\ 0 & 0 & 0 & 1 \\ 1 & 0 & 0 & 0 \\ 0 & 1 & 0 & 0 \end{bmatrix},$$

$$\text{and} \qquad \hat{\tau}_3 = \begin{bmatrix} 0 & 0 & 0 & 1 \\ 0 & 0 & 1 & 0 \\ 0 & 1 & 0 & 0 \\ 1 & 0 & 0 & 0 \end{bmatrix}. \tag{3}$$

Thereby, the hopping parameter represents $t = \hbar^2/(2ma^2)$, where m refers to the effective quasiparticle masses. For our mostly to a qualitative level restricted modeling, it is most convenient to use such units that $t = 1$ [arb.units].

Apart from the discrete single-particle energies $\varepsilon(i, j) = 4t\hat{\tau}_0$ and the ferromagnetic exchange gap $\Delta_{\mathrm{Ni}}^{\mathrm{XC}}$ of Ni (the magnetization vector points along the $\hat{z}$-direction), we need to account for the films' distinct superconducting gaps. The Bogoliubov–de Gennes Hamiltonian involves now not only singlet superconducting gaps (pairing potentials), coupling spin-up and spin-down electrons to form *spin-singlet Cooper pairs*, but also triplet gaps (pairing potentials) that facilitate *spin-triplet Cooper pairs* consisting of two equal-spin electrons. While the *singlet* superconducting gaps are abbreviated by $\Delta_{\mathrm{Al}}^{\mathrm{singlet}}$ and $\Delta_{\mathrm{Ni-Ga}}^{\mathrm{singlet}}$, the

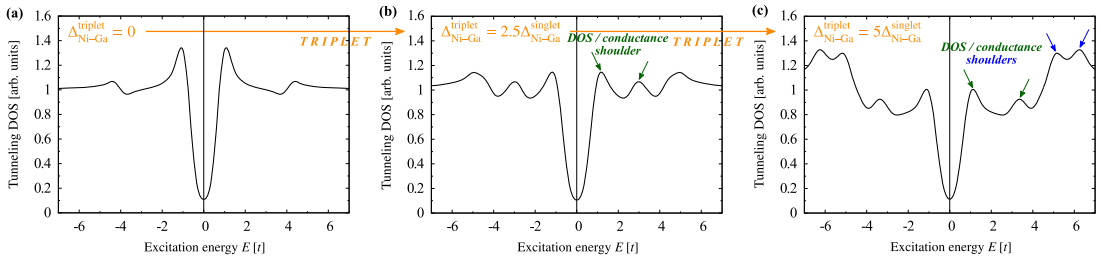

Figure 10. The *calculated* zero-temperature tunneling DOS of the Al ($L_{\text{Al}} = 400$)/Ni ($L_{\text{Ni}} = 160$)–Ga ($L_{\text{Ga}} = 3000$) junction (a) in the absence of interfacial triplet pairing ($\Delta^{\text{triplet}}_{\text{Ni–Ga}} = 0$), (b) in the presence of moderate triplet pairing ($\Delta^{\text{triplet}}_{\text{Ni–Ga}} = 2.5\Delta^{\text{singlet}}_{\text{Ni–Ga}}$), and (c) in the presence of strong triplet pairing ($\Delta^{\text{triplet}}_{\text{Ni–Ga}} = 5\Delta^{\text{singlet}}_{\text{Ni–Ga}}$) in $L'_{\text{Ni}} = L_{\text{Ni}}/4$ and $L'_{\text{Ga}} = L_{\text{Ga}}/4$ of the lattice sites around the Ni–Ga interface. The particular choice of L'_{Ni} and L'_{Ga} is not essential to reproduce the qualitative DOS modulations, as long as $L'_{\text{Ni}} \ll L_{\text{Ni}}$ and $L'_{\text{Ga}} \ll L_{\text{Ga}}$.

triplet gap is denoted by $\Delta^{\text{triplet}}_{\text{Ni–Ga}}$. To ensure that triplet correlations really only occur in the vicinity of the Ni–Ga interface, their respective pairing-potential terms are *nonzero only* in L'_{Ni} and L'_{Ga} of Ni's and Ga's lattice sites around the Ni–Ga interface, as we schematically illustrate in figure 9(b).

Since the inhomogeneous magnetization at the Ni–Ga interfaces, which ultimately induces the triplet pairings we are interested in, stems from a highly complex inhomogeneous magnetic domain structure that has not yet been fully understood at the microscopic level, we manually introduce the interfacial triplet pairings into our toy model through including nonzero tunable equal-spin superconducting pairing terms around the Ni–Ga interface. While this is sufficient to unravel the physical origin of the observed conductance shoulders, more comprehensive, and at the same time more realistic from a microscopic point of view, modeling is certainly desirable at a later stage, after gaining more experimental insight into the magnetic texture at the interface and possibly assisted by first-principles band-structure calculations [114–116].

To proceed, we implement the tight-binding Bogoliubov–de Gennes Hamiltonian, given by equation (1), in Kwant, and use Kwant's internal Kernel polynomial method (KPM) to extract the junctions' spatially integrated zero-temperature tunneling DOS (normalized to its normal-state counterpart) that we essentially probe through our conductance measurements. Along the transverse direction, we include $W = 500$ lattice sites. Although changing W does not qualitatively impact the tunneling DOS (for that reason, we could also completely neglect the third spatial orientation, i.e., the $\hat{x}$-direction, in our junctions), using rather large numbers is reasonable to minimize numerical errors, which might cause unphysical numerical fluctuations in the DOS data.

3.2. Tunneling-DOS simulations and large-bias conductance shoulders

Figure 10 illustrates the computed tunneling DOS of the Al/Ni–Ga junction with the lattice-site numbers $L_{\text{Al}} = 400$, $L_{\text{Ni}} = 160$, and $L_{\text{Ga}} = 3000$; note that these were chosen such that their ratio $L_{\text{Al}} : L_{\text{Ni}} : L_{\text{Ga}} = 400 : 160 : 3000$ matches the film-thickness ratio $d_{\text{Al}} : d_{\text{Ni}} : d_{\text{Ga}} = 4\ \text{nm} : 1.6\ \text{nm} : 30\ \text{nm}$ of sample B, although one cannot directly compare the theoretical and experimental dimensions as we chose $a = 1$ [arb.units] as the lattice constant in our Kwant simulations. The specific values substituted for the singlet superconducting gaps of the Al film and the Ni–Ga bilayer are not particularly relevant to the results; we kept them at $\Delta^{\text{singlet}}_{\text{Al}} = 0.20t$ and $\Delta^{\text{singlet}}_{\text{Ni–Ga}} = 0.80t$ in order to scale their ratio $\Delta^{\text{singlet}}_{\text{Ni–Ga}}/\Delta^{\text{singlet}}_{\text{Al}} = 4$ roughly according to the experimentally from sample A extracted gaps. The amplitude of the superconducting triplet gap, which is only present in the vicinity of the Ni–Ga interface, was initially increased from $\Delta^{\text{triplet}}_{\text{Ni–Ga}} = 0$ (*no triplet pairing*) to $\Delta^{\text{triplet}}_{\text{Ni–Ga}} = 2.5\Delta^{\text{singlet}}_{\text{Ni–Ga}}$ (*moderate triplet pairing*), and finally to $\Delta^{\text{triplet}}_{\text{Ni–Ga}} = 5\Delta^{\text{singlet}}_{\text{Ni–Ga}}$ (*strong triplet pairing*). Enhancing the triplet-pairing strength in our model corresponds to produce a more inhomogeneously magnetized interface domain texture in the experiment, which is expected to occur—coinciding with our experimental results—when decreasing the Ni(–Ga bilayer) thickness to get a rougher interface.

Despite the particular values of triplet gaps substituted into our calculations may seem exaggeratedly large when compared to their singlet counterparts, we can still use them in our numerical simulations to develop a *qualitative* understanding of the underlying physics. One of the reasons that such large triplet gaps are required to reproduce the experimental findings could be the fact that we did not take care of formulating the full model using physically realistic units (recall that we set, for instance, $a = 1$ [arb.units]). Furthermore, and as we mentioned earlier, the triplet-pairing mechanisms in the real samples are a consequence of complex nonuniform interface magnetizations and are therefore at the microscopic level

much more complicated to properly describe than in our strongly simplified phenomenological model. The 'effectiveness' of induced triplet pairings depends additionally also on the strength of ferromagnetism inside the magnetic junction films. We assumed an extremely small exchange energy gap in Ni of $\Delta_{\mathrm{Ni}}^{\mathrm{XC}} = 0.5t$—when compared to the singlet superconducting gaps, which are typically orders of magnitude smaller than ferromagnetic exchange couplings—in our simulations to demonstrate that even extremely weak ferromagnetism suffices to observe transport ramifications of superconducting triplet pairings. Considering a typical metal Fermi level $\mu \approx 10^3 \Delta_{\mathrm{Ni-Ga}}^{\mathrm{singlet}}$, $\Delta_{\mathrm{Ni}}^{\mathrm{XC}} = 0.5t$ corresponds to a Ni spin polarization of just $\mathcal{P}_{\mathrm{Ni}} = (\Delta_{\mathrm{Ni}}^{\mathrm{XC}}/2)/\mu \approx 0.03\,\%$. Although Meservey–Tedrow spectroscopy indicated that the Ni spin polarization in our samples is only about 1%, this is still notably larger than the tiny value assumed for our simulations, which could provide another reason for the large effective triplet pairings required in our simulations to recover the experimentally evident features.

In the absence of triplet pairing at the Ni–Ga interface, we recover two DOS maxima (becoming visible in our transport measurements in terms of conductance maxima) that we associated with the energies of the singlet superconducting gaps of Al and the Ni–Ga bilayer when analyzing the experimental data obtained from sample A (recall the Rowell–Feldman description explained in section 2). Already moderate triplet pairing, however, turns the first DOS maximum at the lower of the two bias voltages into two neighboring maxima, and thereby forms the first shoulder that we probably witnessed in the conductance spectrum of sample B. The second experimentally observed shoulder at slightly larger bias voltage eventually appears when the triplet-pairing strength is further enhanced. The latter shoulder (i.e., the one at larger bias voltage) seems to be less sensitive to interfacial triplet pairings in general since the splitting between its two neighboring conductance maxima is substantially smaller than that within the first—in good agreement with our experimental results (recall the conductance data of samples B and C presented in figure 3)—and requires thus a more sizable triplet-pairing strength to become indeed evident. *Although our theoretical DOS simulations are robust enough to qualitatively demonstrate that the experimentally detected large-bias conductance shoulders indeed provide a transport fingerprint of triplet pairings at the Ni–Ga bilayer interface, theory and experiment can, at least at this point, not be compared to each other at the quantitative level due to the strong simplifications made in our model.*

4. Conclusions

In summary, we thoroughly discussed and analyzed our tunneling-conductance measurements on superconducting magnetic Al/Al_2O_3(/EuS)/Ni–Ga junctions, focusing, in particular, on thicker Ni (3 nm)–Ga (60 nm) and thinner Ni (1.6 nm)–Ga (30 nm) bilayers, respectively. While the conductance spectrum in the first case could be explained based on the findings of earlier studies, the second scenario turned out to become much more puzzling, as it mainly led to the additional formation of unexpected large-bias conductance shoulders that have not yet been understood. Since the latter remained mostly unaffected when 'inverting' the Ni and Ga films, we concluded that all important physics should happen near the Ni–Ga interface.

Performing PNR analyses to collect more information about the structure and magnetization of this interface, we detected the paramagnetic Meissner response in Ga to convince that the proximity-coupled bilayer induces superconducting triplet pairings around the Ni–Ga interface. With this in mind, we elaborated on a strongly simplified theoretical toy model, which allowed us to compute the junctions' tunneling DOS that our conductance measurements essentially probe. Comparing our phenomenological DOS simulations with experimental conductance data substantiated that the conductance shoulders do indeed provide a well-accessible transport fingerprint of newly induced superconducting triplet correlations in the vicinity of the Ni–Ga interface.

To further characterize the novel triplet pairings within the Ni–Ga bilayer, we suggest to subsequently analyze the Ni–Ga-interface profile through SQUID and Lorentz-microscopy measurements, which can directly probe inhomogeneous spin textures around the interface. Moreover, investigating our samples' transport characteristics in the presence of an external magnetic field might give deeper insight into the triplet-pairing mechanism, as this manipulates the inhomogeneity of the interface magnetizations and shall therefore give a unique magnetization dependence to the conductance shoulders.

Acknowledgments

The experimental work performed in the US was supported by the NSF C-Accel. Track C under Grant No. 2040620, NSF Grant DMR 1700137, ONR Grants N00014-16-1-2657 and N00014-20-1-2306, and John Templeton Foundation Grants 39944 and 60148. The theoretical work at the University of Regensburg (AC and JF) received funding from the Elite Network of Bavaria through the International Doctorate

Program Topological Insulators, and Deutsche Forschungsgemeinschaft (DFG, German Research Foundation) through Subproject B07 within the Collaborative Research Center SFB 1277 (Project-ID 314695032) and the Research Grant 'Spin and magnetic properties of superconducting tunnel junctions' (Project-ID 454646522). The undergraduate MS was supported by the UROP program funds at Massachusetts Institute of Technology. This research used resources at the Spallation Neutron Source, a DOE Office of Science User Facility operated by the Oak Ridge National Laboratory.

Data availability statement

The data that support the findings of this study are available upon reasonable request from the authors.

ORCID iDs

Andreas Costa https://orcid.org/0000-0001-5706-2198
Valeria Lauter https://orcid.org/0000-0003-0989-6563
Jaroslav Fabian https://orcid.org/0000-0002-3009-4525
Jagadeesh S Moodera https://orcid.org/0000-0002-2480-1211

References

[1] Žutić I, Fabian J and Das Sarma S 2004 *Rev. Mod. Phys.* **76** 323–410
[2] Fabian J, Matos-Abiague A, Ertler C, Stano P and Žutić I 2007 *Acta Phys. Slovaca* **57** 565–907
[3] Eschrig M 2011 *Phys. Today* **64** 43–9
[4] Linder J and Robinson J W A 2015 *Sci. Rep.* **5** 15483
[5] Ohnishi K, Komori S, Yang G, Jeon K-R, Olde Olthof L A B, Montiel X, Blamire M G and Robinson J W A 2020 *Appl. Phys. Lett.* **116** 130501
[6] Ioffe L B, Geshkenbein V B, Feigel'man M V, Fauchère A L and Blatter G 1999 *Nature* **398** 679–81
[7] Mooij J E, Orlando T P, Levitov L, Tian L, van der Wal C H and Lloyd S 1999 *Science* **285** 1036
[8] Blatter G, Geshkenbein V B and Ioffe L B 2001 *Phys. Rev.* B **63** 174511
[9] Ustinov A V and Kaplunenko V K 2003 *J. Appl. Phys.* **94** 5405
[10] Yamashita T, Tanikawa K, Takahashi S and Maekawa S 2005 *Phys. Rev. Lett.* **95** 097001
[11] Feofanov A K *et al* 2010 *Nat. Phys.* **6** 593
[12] Khabipov M I, Balashov D V, Maibaum F, Zorin A B, Oboznov V A, Bolginov V V, Rossolenko A N and Ryazanov V V 2010 *Supercond. Sci. Technol.* **23** 045032
[13] Devoret M H and Schoelkopf R J 2013 *Science* **339** 1169–74
[14] Soulen R J Jr *et al* 1998 *Science* **282** 85–8
[15] Soulen R J Jr *et al* 1999 *J. Appl. Phys.* **85** 4589–91
[16] de Jong M J M and Beenakker C W J 1995 *Phys. Rev. Lett.* **74** 1657–60
[17] Golubov A A, Kupriyanov M Y and Il'ichev E 2004 *Rev. Mod. Phys.* **76** 411–69
[18] Yu Luh L 1965 *Acta Phys. Sin.* **21** 75–91
[19] Shiba H 1968 *Prog. Theor. Phys.* **40** 435–51
[20] Rusinov A I 1968 *Zh. Eksp. Teor. Fiz. Pisma Red.* **9** 146
Rusinov A I 1969 *JETP Lett.* **9** 85 (Engl. transl.)
[21] Costa A, Fabian J and Kochan D 2018 *Phys. Rev.* B **98** 134511
[22] Kochan D, Barth M, Costa A, Richter K and Fabian J 2020 *Phys. Rev. Lett.* **125** 087001
[23] Bulaevskii L N, Kuzii V V and Sobyanin A A 1977 *Pis'ma Zh. Eksp. Teor. Fiz.* **25** 314–8
Bulaevskii L N, Kuzii V V and Sobyanin A A 1977 *JETP Lett.* **25** 290 (Engl. transl.)
[24] Ryazanov V V, Oboznov V A, Rusanov A Y, Veretennikov A V, Golubov A A and Aarts J 2001 *Phys. Rev. Lett.* **86** 2427–30
[25] Nilsson J, Akhmerov A R and Beenakker C W J 2008 *Phys. Rev. Lett.* **101** 120403
[26] Duckheim M and Brouwer P W 2011 *Phys. Rev.* B **83** 054513
[27] Lee S-P, Alicea J and Refael G 2012 *Phys. Rev. Lett.* **109** 126403
[28] Nadj-Perge S, Drozdov I K, Li J, Chen H, Jeon S, Seo J, MacDonald A H, Bernevig B A and Yazdani A 2014 *Science* **346** 602–7
[29] Dumitrescu E, Roberts B, Tewari S, Sau J D and Das Sarma S 2015 *Phys. Rev.* B **91** 094505
[30] Pawlak R, Kisiel M, Klinovaja J, Meier T, Kawai S, Glatzel T, Loss D and Meyer E 2016 *npj Quantum Inf.* **2** 16035
[31] Ruby M, Heinrich B W, Peng Y, von Oppen F and Franke K J 2017 *Nano Lett.* **17** 4473–7
[32] Livanas G, Sigrist M and Varelogiannis G 2019 *Sci. Rep.* **9** 6259
[33] Manna S, Wei P, Xie Y, Law K T, Lee P A and Moodera J S 2020 *Proc. Natl Acad. Sci. USA* **117** 8775–82
[34] Högl P, Matos-Abiague A, Žutić I and Fabian J 2015 *Phys. Rev. Lett.* **115** 116601
[35] Högl P, Matos-Abiague A, Žutić I and Fabian J 2015 *Phys. Rev. Lett.* **115** 159902
[36] Jacobsen S H, Kulagina I and Linder J 2016 *Sci. Rep.* **6** 23926
[37] Costa A, Högl P and Fabian J 2017 *Phys. Rev.* B **95** 024514
[38] Martínez I *et al* 2020 *Phys. Rev. Appl.* **13** 014030
[39] Keizer R S, Goennenwein S T B, Klapwijk T M, Miao G, Xiao G and Gupta A 2006 *Nature* **439** 825–7
[40] Moodera J S and Meservey R 1990 *Phys. Rev.* B **42** 179
[41] LeClair P, Moodera J S, Philip J and Heiman D 2005 *Phys. Rev. Lett.* **94** 037006
[42] Belzig W, Bruder C and Schön G 1996 *Phys. Rev.* B **53** 5727–33
[43] Kadigrobov A, Shekhter R I and Jonson M 2001 *Europhys. Lett.* **54** 394–400
[44] Bergeret F S, Volkov A F and Efetov K B 2001 *Phys. Rev. Lett.* **86** 4096–9
[45] Bergeret F S, Volkov A F and Efetov K B 2005 *Rev. Mod. Phys.* **77** 1321–73

[46] Yokoyama T, Tanaka Y and Golubov A A 2007 *Phys. Rev.* B **75** 134510
[47] Linder J, Yokoyama T, Sudbø A and Eschrig M 2009 *Phys. Rev. Lett.* **102** 107008
[48] Khaire T S, Khasawneh M A, Pratt W P Jr and Birge N O 2010 *Phys. Rev. Lett.* **104** 137002
[49] Robinson J W A, Witt J D S and Blamire M G 2010 *Science* **329** 59–61
[50] Anwar M S, Czeschka F, Hesselberth M, Porcu M and Aarts J 2010 *Phys. Rev.* B **82** 100501
[51] Yokoyama T, Tanaka Y and Nagaosa N 2011 *Phys. Rev. Lett.* **106** 246601
[52] Bergeret F S, Verso A and Volkov A F 2012 *Phys. Rev.* B **86** 060506
[53] Bergeret F S and Tokatly I V 2013 *Phys. Rev. Lett.* **110** 117003
[54] Bergeret F S and Tokatly I V 2014 *Phys. Rev.* B **89** 134517
[55] Alidoust M, Halterman K and Valls O T 2015 *Phys. Rev.* B **92** 014508
[56] Di Bernardo A, Diesch S, Gu Y, Linder J, Divitini G, Ducati C, Scheer E, Blamire M G and Robinson J W A 2015 *Nat. Commun.* **6** 8053
[57] Arjoranta J and Heikkilä T T 2016 *Phys. Rev.* B **93** 024522
[58] Espedal C, Yokoyama T and Linder J 2016 *Phys. Rev. Lett.* **116** 127002
[59] Pal A, Ouassou J A, Eschrig M, Linder J and Blamire M G 2017 *Sci. Rep.* **7** 3–7
[60] Bergeret F S and Tokatly I V 2020 *Phys. Rev.* B **102** 060506
[61] Bergeret F S, Volkov A F and Efetov K B 2001 *Phys. Rev. Lett.* **86** 3140–3
[62] Bergeret F S, Volkov A F and Efetov K B 2001 *Phys. Rev.* B **64** 134506
[63] Eschrig M, Kopu J, Cuevas J C and Schön G 2003 *Phys. Rev. Lett.* **90** 137003
[64] Houzet M and Buzdin A I 2007 *Phys. Rev.* B **76** 060504
[65] Eschrig M and Löfwander T 2008 *Nat. Phys.* **4** 138–43
[66] Grein R, Eschrig M and Schön G 2009 *Phys. Rev. Lett.* **102** 227005
[67] Robinson J W A, Halász G B, Buzdin A I and Blamire M G 2010 *Phys. Rev. Lett.* **104** 207001
[68] Banerjee N, Robinson J W A and Blamire M G 2014 *Nat. Commun.* **5** 1–6
[69] Diesch S, Machon P, Wolz M, Sürgers C, Beckmann D, Belzig W and Scheer E 2018 *Nat. Commun.* **9** 5248
[70] Satchell N and Birge N O 2018 *Phys. Rev.* B **97** 214509
[71] Satchell N, Loloee R and Birge N O 2019 *Phys. Rev.* B **99** 174519
[72] Eskilt J R, Amundsen M, Banerjee N and Linder J 2019 *Phys. Rev.* B **100** 224519
[73] Bujnowski B, Biele R and Bergeret F S 2019 *Phys. Rev.* B **100** 224518
[74] Machida K and Klemm R A 1978 *Solid State Commun.* **27** 1061–3
[75] Alidoust M, Halterman K and Linder J 2014 *Phys. Rev.* B **89** 054508
[76] Asano Y, Fominov Y V and Tanaka Y 2014 *Phys. Rev.* B **90** 094512
[77] Di Bernardo A *et al* 2015 *Phys. Rev.* X **5** 041021
[78] Rouco M, Chakraborty S, Aikebaier F, Golovach V N, Strambini E, Moodera J S, Giazotto F, Heikkilä T T and Bergeret F S 2019 *Phys. Rev.* B **100** 184501
[79] Meservey R and Tedrow P M 1994 *Phys. Rep.* **238** 173–243
[80] Tedrow P M and Meservey R 1971 *Phys. Rev. Lett.* **26** 192–5
[81] Tedrow P M and Meservey R 1973 *Phys. Rev.* B **7** 318–26
[82] Taylor B N and Burstein E 1963 *Phys. Rev. Lett.* **10** 14–7
[83] Adkins C J 1963 *Phil. Mag.* **8** 1051–61
[84] Adkins C J 1964 *Rev. Mod. Phys.* **36** 211–3
[85] van Huffelen W M, Klapwijk T M, Heslinga D R, de Boer M J and van der Post N 1993 *Phys. Rev.* B **47** 5170–89
[86] Kuhlmann M, Zimmermann U, Dikin D, Abens S, Keck K and Dmitriev V M 1994 *Z. Phys.* B **96** 13–24
[87] Zimmermann U, Abens S, Dikin D, Keck K and Dmitriev V M 1995 *Z. Phys.* B **97** 59–66
[88] Rowell J M 1964 *Rev. Mod. Phys.* **36** 199–200
[89] Rowell J M and Feldmann W L 1968 *Phys. Rev.* **172** 393–401
[90] Klapwijk T M, Blonder G E and Tinkham M 1982 *Physica B+C* **109–110** 1657
[91] Octavio M, Tinkham M, Blonder G E and Klapwijk T M 1983 *Phys. Rev.* B **27** 6739–46
[92] Flensberg K, Hansen J B and Octavio M 1988 *Phys. Rev.* B **38** 8707–11
[93] Arnold G B 1985 *J. Low Temp. Phys.* **59** 143–83
[94] Arnold G B 1987 *J. Low Temp. Phys.* **68** 1–27
[95] Costa A and Fabian J 2021 *Phys. Rev.* B **104** 174504
[96] Guéron S, Pothier H, Birge N O, Esteve D and Devoret M H 1996 *Phys. Rev. Lett.* **77** 3025–8
[97] Pothier H, Guéron S, Birge N O, Esteve D and Devoret M H 1997 *Phys. Rev. Lett.* **79** 3490–3
[98] Kalcheim Y, Millo O, Di Bernardo A, Pal A and Robinson J W A 2015 *Phys. Rev.* B **92** 060501
[99] Ouassou J A, Pal A, Blamire M, Eschrig M and Linder J 2017 *Sci. Rep.* **7** 1932
[100] Alidoust M and Halterman K 2018 *Phys. Rev.* B **97** 064517
[101] Halterman K and Alidoust M 2018 *Phys. Rev.* B **98** 134510
[102] Alidoust M and Halterman K 2020 *Phys. Rev.* B **102** 224504
[103] Moodera J S, Hao X, Gibson G A and Meservey R 1988 *Phys. Rev. Lett.* **61** 637–40
[104] Strambini E, Golovach V N, De Simoni G, Moodera J S, Bergeret F S and Giazotto F 2017 *Phys. Rev. Mater.* **1** 054402
[105] De Simoni G, Strambini E, Moodera J S, Bergeret F S and Giazotto F 2018 *Nano Lett.* **18** 6369–74
[106] Lauter-Pasyuk V 2007 *Collect. Soc. Fr. Neutron* **7** s221–40
[107] Lauter-Pasyuk V, Lauter H J, Aksenov V L, Kornilov E I, Petrenko A V and Leiderer P 1998 *Physica* B **248** 166–70
[108] Lauter-Pasyuk V, Lauter H J, Lorenz M, Aksenov V L and Leiderer P 1999 *Physica* B **267–268** 149–53
[109] Devizorova Z, Mironov S V, Mel'nikov A S and Buzdin A 2019 *Phys. Rev.* B **99** 104519
[110] Lauter V, Ambaye H, Goyette R, Hal Lee W-T and Parizzi A 2009 *Physica* B **404** 2543–6
[111] Lauter-Pasyuk V, Lauter H J, Lorenz M, Petrenko A, Nikonov O, Aksenov V L and Leiderer P 2000 *Physica* B **276–278** 776–7
[112] De Gennes P G 1989 *Superconductivity of Metals and Alloys* (Reading, MA: Addison-Wesley)
[113] Groth C W, Wimmer M, Akhmerov A R and Waintal X 2014 *New J. Phys.* **16** 063065
[114] Csire G, Újfalussy B and Annett J F 2018 *Eur. Phys. J.* B **91** 217
[115] Csire G, Deák A, Nyári B, Ebert H, Annett J F and Újfalussy B 2018 *Phys. Rev.* B **97** 024514
[116] Gmitra M, Matos-Abiague A, Draxl C and Fabian J 2013 *Phys. Rev. Lett.* **111** 036603